Journal of the European Ceramic Society 22 (2002) 1839–1846

www.elsevier.com/locate/jeurceramsoc

Subsolidus phase relations in the SnO_2–$CuSb_2O_6$ binary system

Oana Scarlat*, Maria Susana-Mihaiu, Maria Zaharescu

Romanian Academy, Institute of Physical Chemistry "I. G. Murgulescu", 202 Splaiul Independentei, 77208 Bucharest 6, Romania

Received 8 June 2001; received in revised form 17 October 2001; accepted 11 November 2001

Abstract

The SnO_2–$CuSb_2O_6$ binary system plays a significant role in the SnO_2–Sb_2O_3–CuO ternary system, delimiting the compositional ranges and their sensor and catalytic properties. The initial compositions expressed as $(1-x)$ SnO_2–$xCuSb_2O_6$ were treated both non-isothermally using DTA up to 1500 °C and iso-thermally at temperatures between 1000 and 1200 °C. Phase analysis of the samples was determined by XRD and IR spectroscopy. It was established that SnO_2–$CuSb_2O_6$ is a pseudobinary system with a solid solubility limit of the end members. The determined lattice parameters of the unit cell of the obtained rutile and trirutile solid solutions obeyed Vegard's rule. From IR spectral investigations it was inferred that Sn^{4+} might be preferentially incorporated on Sb^{5+} sites into the $CuSb_2O_6$ lattice.

Keywords: $CuSb_2O_6$; Powders; SnO_2; Solid state reaction; Structural applications; X-ray methods

1. Introduction

In the past few decades there has been a growing interest in the use of SnO_2-based ceramics, due to their specific electrical properties and high temperature stability.[1,2] A considerable amount of current research activities has been devoted to the development of stable tin dioxide based catalytic materials. Part of these studies, the SnO_2–Sb_2O_3 system, has been evidenced to be a binary system, with a solid solubility limit of the components. In this respect, the addition of Sb_2O_3 is claimed to enhance drastically by four to five orders of magnitude the electrical conductivity of SnO_2.[1]

However, the sintering capability of the SnO_2–Sb_2O_3 is very poor. As evidenced by previous studies, the addition of CuO has significantly improved the densification properties of these SnO_2[1,2] based materials. The electrical resistivity of the SnO_2–CuO binary compositions proved to present high sensitivity to traces of most of the toxic and flammable gases. Accordingly, SnO_2-rich compositions were extensively studied and only in the subsolidus domain, which is important for sensor applications.[3,4] Our recent results indicate that over 1030 °C, there are evidences for the transformation of the SnO_2–CuO initial binary system into the pseudo-ternary SnO_2–CuO–Cu_2O.[5]

In a recent study concerning the phase relationships of the Sb_2O_3–CuO binary system, the formation of the $CuO{\cdot}Sb_2O_5$ ($CuSb_2O_6$) binary compound containing pentavalent antimony, has been reported.[6] Bystrom et al. has identified its structure in an earlier work,[7] as belonging to the *monoclinic* system with a high tendency to adopt a tetragonal symmetry, due to the presence of the Cu^{2+} ion. In some special conditions, two other binary compounds $9CuO{\cdot}2Sb_2O_5$[8,9] and $4Cu_2O{\cdot}Sb_2O_5$ ($Cu_8Sb_2O_9$),[10] with high copper content have been prepared, but no crystallographic data about the structure was reported.

Our previous papers[11,12] concerning the oxide materials from the SnO_2–Sb_2O_3–CuO ternary system, pointed out the complexity of the solid state reactions taking place at different temperatures as follows:

$$\approx 500\ ^\circ\mathrm{C}: \quad Sb_2O_3 + 1/2O_2 \rightarrow Sb_2O_4 \tag{1}$$

$$< 900\ ^\circ\mathrm{C}: \quad Sb_2O_4 + CuO + 1/2O_2 \rightarrow CuSb_2O_6 \tag{2}$$

$$940\ ^\circ\mathrm{C}: \quad CuSb_2O_6 + 7CuO \rightarrow 2Cu_8Sb_2O_9 + 2O_2 \tag{3}$$

$$1100\ ^\circ\mathrm{C}: \quad SnO_2 + Sb_2O_4 + CuSb_2O_6 \rightarrow SnO_{2\ ss} \tag{4}$$

* Corresponding author.
E-mail address: ioana@chimfiz.icf.ro (O. Scarlat).

0955-2219/02/$ - see front matter
PII: S0955-2219(01)00507-6

The Cu–Sb–O model for composition modifications[13] has lead to a quaternary oxide representation of the Sn–Sb–Cu–O subsolidus phase equilibrium. Moreover, considering the experimental confirmations of the weight changes of the SnO_2–Sb_2O_3–CuO ternary compositions, the resulted domains of the phase equilibria might be graphically presented for a temperature of 1100 °C, as in Fig. 1. Two types of solid solutions: $SnO_{2\ ss}$ and $CuSb_2O_{6\ ss}$ respectively, have been evidenced in this system.[14] In the subsolidus domain, the formation of the $CuSb_2O_6$ binary compound, which precedes the formation as a unique phase, of the tin dioxide based solid solution, with *rutile* type structure ($SnO_{2\ ss}$), was found to be a basic stage in the SnO_2–Sb_2O_3–CuO ternary system evolution. Because the compositions close to the $CuSb_2O_6$ binary compound were less investigated in previous studies,[14] the limits of different phases and solid solutions coexistence have not been precisely established.

A thorough study of the SnO_2–$CuSb_2O_6$ binary system was considered to be representative for the study of the Sn–Sb–Cu–O initial system.

In this work, phase equilibria involving the oxide phases between SnO_2 and $CuSb_2O_6$ were determined by isothermal equilibration and phase analysis of the samples, covering the whole concentration range. To elucidate the geometry and electronic structure of [CuO_6] polyhedra with dependence on $x_{CuSb_2O_6}$, IR spectroscopic investigations have been performed.

2. Experimental procedure

The studied mixtures were prepared by classical ceramic method[1,14] using commercially available SnO_2, Sb_2O_3, CuO (Merck Co.). The interoxide $CuSb_2O_6$ binary compound was prepared and characterized in the laboratory from an equimolar mixture of CuO and Sb_2O_3, in accordance with our previous results.[12]

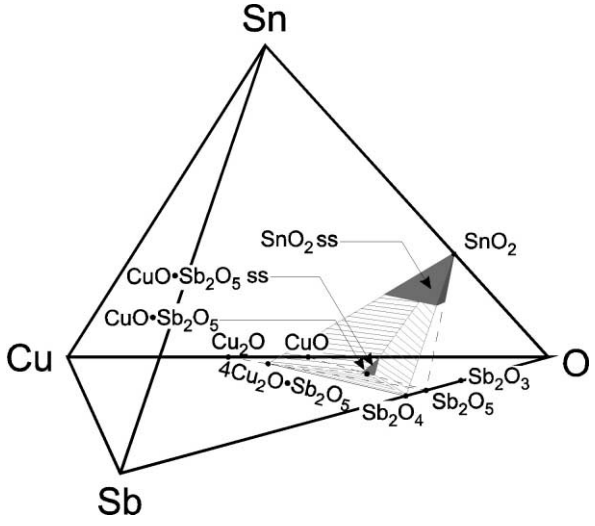

Fig. 1. Sn–Sb–Cu–O quaternary system. Subsolidus phase domains at 1000 °C.

The studied compositions are expressed as $(1-x)$ SnO_2–$xCuSb_2O_6$ with $x = 0$, 0.1, 0.2, 0.25, ... 0.75, 0.8, ...1, covering the whole concentration range.

The stability at high temperatures of the mixtures was studied up to 1500 °C by thermal analysis using a Perkin Elmer Instrument—Pyris 7 differential thermal analyzer. For each sample the platinum reference pan was loaded with an amount of alumina powder equal to the weight of the powder in the sample pan. All TA tests were performed with heating rates of 2 °C/min and cooling rates of 5 °C/min in air. Weight losses associated with the various transformations were observed using a Perkin Elmer Instrument—Pyris 7 Thermogravimetric Analyzer.

Disc samples (10 mm diameter and ~2 g in weight) were made by uniaxial pressing at 30 MPa followed by thermal treatments at temperatures between 1000 and 1200 °C—holding times of max. 10 h.

For phase determination, X-ray step scans (0.01° step size, 2.5 s counting time) over the range 10–80 °2θ, were performed on the resulted powders from the grounded pellets. A Scintag automated diffractometer fitted with a solid state counter, working with CuK_α radiation ($\lambda_{K\alpha 1} = 1.54059$ Å), have been used.

IR spectra of the obtained phases were carried out with a Specord M 80 type Carl Zeiss Jena IR Spectrometer recorded in the 1100–200 cm^{-1} spectral range (with a resolution of 4 cm^{-1}), a wave number domain typical for the IR absorption properties of oxide materials. Using the KBr pellets technique, 0.9 mg of sample were mixed with 200 mg of KBr (KBr for Spectroscopy Uvasol, Merck, Germany). Due to the KBr infrared absorption properties, the recorded absorption bands placed at lower frequencies (i.e. 350–200 cm^{-1}) are on a doubtful accuracy, a fact which limited the actual investigated spectral range down to 350 cm^{-1}.

3. Experimental results

3.1. Studies in non-isothermal conditions

DTA results are presented for some selected samples in Fig. 2. For pure SnO_2 ($x = 0$), no thermal effects were noticed, evidencing its bulk high temperature stability up to 1500 °C. For pure $CuSb_2O_6$ ($x = 1$) and in reasonable agreement with previously published data,[10] own DTA results (Fig. 2) and the derivative of the TG curve presented in Fig. 3, suggest that more than one chemical process developed between 1125 and 1450 °C according to the following reactions:

$$4CuSb_2O_6 \xrightarrow{\approx 1213\ ^\circ C} Cu_4SbO_{4.5} + \frac{7}{2}Sb_2O_3 + \frac{9}{2}O_2 \qquad (5)$$

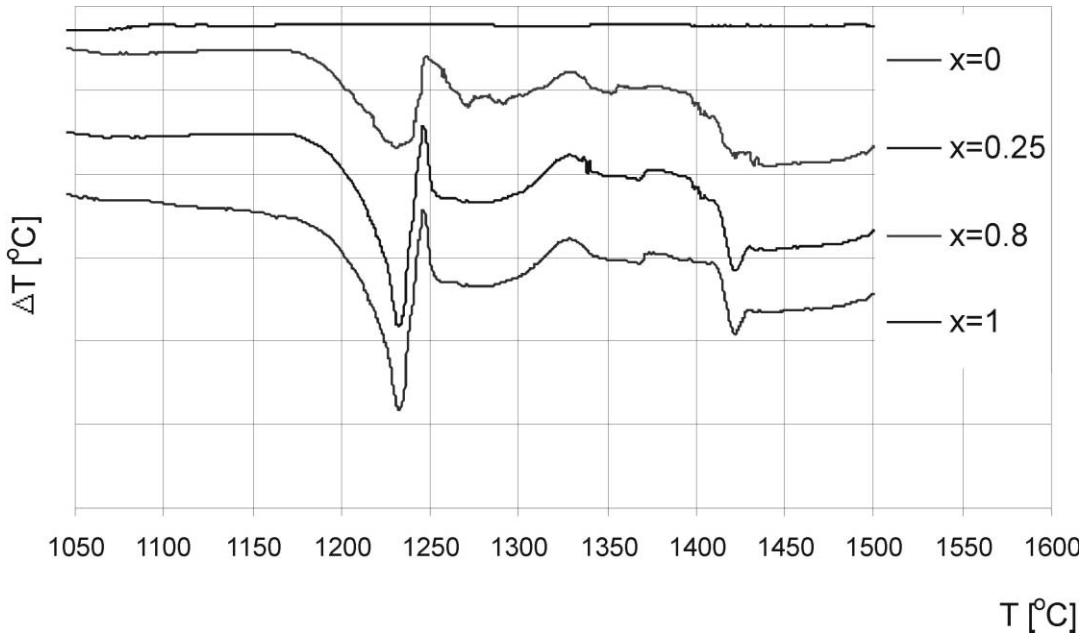

Fig. 2. DTA results for $(1-x)$ SnO_2–$xCuSb_2O_6$ compositions (air, 2 grd/min).

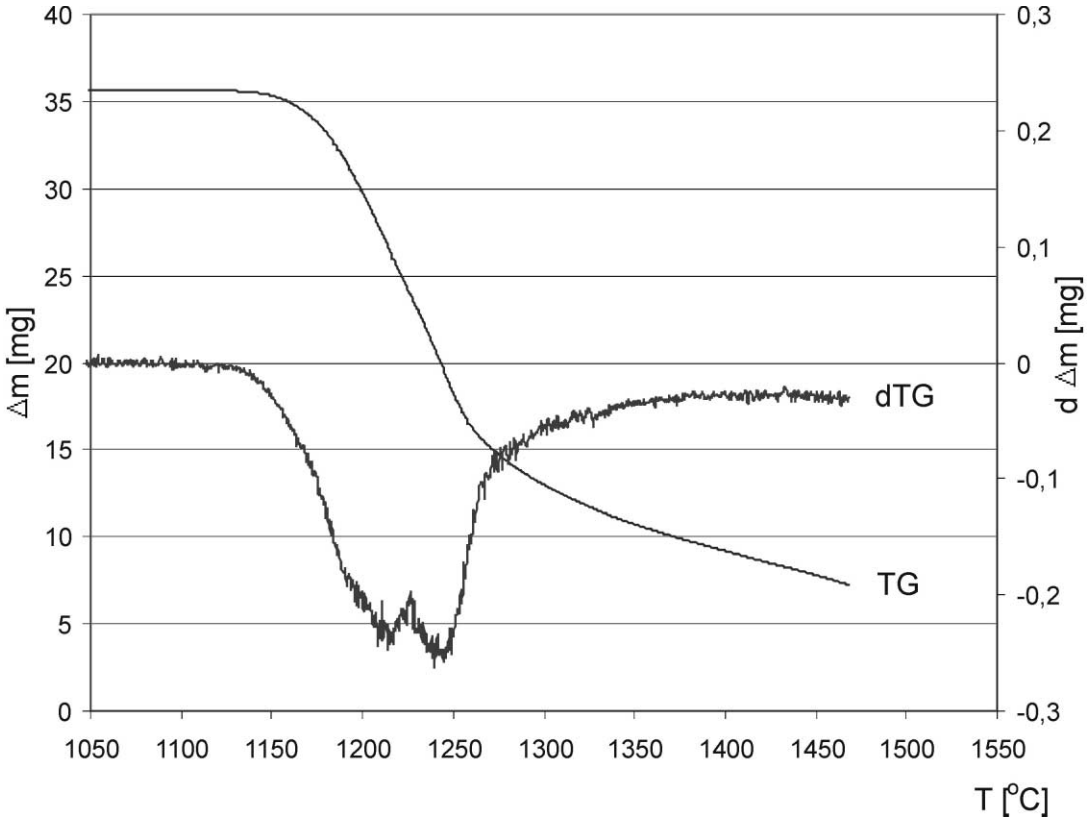

Fig. 3. TGA/dTG results for $CuSb_2O_6$ (air, 2 grd / min).

$$2Cu_4SbO_{4.5} \xrightarrow{\approx 1247\ ^\circ C} 4Cu_2O + Sb_2O_3 + O_2 \quad (6)$$

Up to 1450 °C the system loses weight progressively (Fig. 3). As previously reported by Shimada et al.,[10] the endothermic effects noticed on the corresponding DTA curve (Fig. 2) might be assigned to reactions (5) and (6).

At high temperatures, there are identified in Fig. 2, some supplementary, not well-resolved and broad thermal effects. These ones might be attributed to the processes of

antimony trioxide volatilisation, the reduction of copper oxide, and to the appearance of the liquid phase extending from Cu–O system, all proceeding for temperatures over 1200 °C.[10,15]

As a conclusion, the thermal effects observed on DTA curves of the selected $(1-x)$ SnO_2–$xCuSb_2O_6$ compositions (Fig. 2), are exclusively a result of the presence in the initial mixture of $CuSb_2O_6$. This observation suggests that no solid state interactions have occurred between SnO_2 and $CuSb_2O_6$ in non-isothermal conditions.

3.2. Studies in iso-thermal conditions

The temperatures for iso-thermal treatments of the studied samples were chosen based on the previous reported data[14] and the presented DTA/TG results.

The phase analysis of the thermally treated samples, obtained by XRD, is presented in Table 1. The presence of SnO_2 solid solution ($SnO_{2\ ss}$) and $CuSb_2O_6$ solid solution ($CuSb_2O_{6\ ss}$) as well as of a mixture of these two phases was evidenced.

An increase of the temperature value over 1200 °C, was not possible due to reactions (5) and (6), resulting in the decomposition and partial melting of pure and $CuSb_2O_6$ solid solution.

The formation of $SnO_{2\ ss}$ and $CuSb_2O_{6\ ss}$ is confirmed by the determination of the lattice parameters of the characteristic unit cell, which are presented for the obtained phases in Table 2.

In order to yield supplementary structural information on the obtained solid solutions, IR spectral investigations were carried out. The resulted absorption spectra are presented in Fig. 4.

4. Discussion

4.1. SnO_2 solid solutions

For $SnO_{2\ ss}$, the presumably substitution of Sn^{4+} ($r=0.69$ Å) by Cu^{2+} ($r=0.73$ Å) and Sb^{5+} ($r=0.62$ Å)[16] results in the decrease of the unit cell lattice parameters. For the tin rich-end members of the series, which crystallise with the *rutile* type lattice, in the composition range of P_4^2 mnm structure, the measured a_o [Å] and c_o [Å] lattice parameters obey Vegard's Rule

$$a_0 = 4.736 - 0.0016 \cdot x_{CuSb_2O_6} \pm 0.002\ \text{Å}$$

$$c_0 = 3.1865 - 0.0016 \cdot x_{CuSb_2O_6} \pm 0.002\ \text{Å}$$

The solid solubility limit of $CuSb_2O_6$ in SnO_2 was estimated to be at $x_{CuSb_2O_6} \cong 0.25$, in accordance with previous reported results obtained using SnO_2, CuO and Sb_2O_3 as starting materials.[11] Over this limit value of concentration it has been established that the SnO_2-based lattice parameters remained practically constant.

The formation of $SnO_{2\ ss}$ is confirmed by IR spectral investigations (Fig. 4). In Fig. 4 the IR spectra of pure SnO_2 used as reference, is also presented. For SnO_2 all relevant IR absorption were found to lie within the reported spectral ranges.[17] The 650 cm^{-1} (vs), 620 cm^{-1} (vs), 555 cm^{-1} (s) were the main bands observed. As mentioned before by Xie et al.,[18] the relative intensity of these bands strongly depends on the crystallinity of the specimen, the two bands at higher frequencies being well deconvoluted only at high degrees of crystallinity.

Table 1
Phase composition of the $(1-x)$ SnO_2–$xCuSb_2O_6$ mixtures. Iso-thermal treatment at various temperatures

Nr. Crt	Oxide composition		Temperature (°C)				
	SnO_2	$CuSb_2O_6$	1000			1100	1200
			1 h	3 h	10 h	3 h	3 h
1	1	0	SnO_2	SnO_2	SnO_2	$SnO_{2\ ss}$	$SnO_{2\ ss}$
2	0.96	0.04	SnO_2	SnO_2	SnO_2	$SnO_{2\ ss}$	$SnO_{2\ ss}$
3	0.94	0.06	SnO_2	SnO_2	SnO_2	$SnO_{2\ ss}$	$SnO_{2\ ss}$
4	0.92	0.08	$SnO_2+CuSb_2O_6$	$SnO_2+CuSb_2O_6$	$SnO_2+CuSb_2O_6$	$SnO_{2\ ss}$	$SnO_{2\ ss}$
5	0.90	0.10	$SnO_2+CuSb_2O_6$	$SnO_2+CuSb_2O_6$	$SnO_2+CuSb_2O_6$	$SnO_{2\ ss}$	$SnO_{2\ ss}$
6	0.80	0.20	$SnO_2+CuSb_2O_6$	$SnO_2+CuSb_2O_6$	$SnO_2+CuSb_2O_6$	$SnO_{2\ ss}$	$SnO_{2\ ss}$
7	0.75	0.25	$SnO_2+CuSb_2O_6$	$SnO_2+CuSb_2O_6$	$SnO_2+CuSb_2O_6$	$SnO_{2\ ss}$	$SnO_{2\ ss}+Cu_4SbO_{4.5}$
8	0.70	0.30	$SnO_2+CuSb_2O_6$	$SnO_2+CuSb_2O_6$	$SnO_2+CuSb_2O_6$	$SnO_{2\ ss}+CuSb_2O_{6\ ss}$	$SnO_{2\ ss}+Cu_4SbO_{4.5}$
9	0.60	0.40	$SnO_2+CuSb_2O_6$	$SnO_2+CuSb_2O_6$	$SnO_2+CuSb_2O_6$	$SnO_{2\ ss}+CuSb_2O_{6\ ss}$	$SnO_{2\ ss}+Cu_4SbO_{4.5}$
10	0.50	0.50	$SnO_2+CuSb_2O_6$	$SnO_2+CuSb_2O_6$	$SnO_2+CuSb_2O_6$	$SnO_{2\ ss}+CuSb_2O_{6\ ss}$	$SnO_{2\ ss}+Cu_4SbO_{4.5}$
11	0.40	0.60	$SnO_2+CuSb_2O_6$	$SnO_2+CuSb_2O_6$	$SnO_2+CuSb_2O_6$	$SnO_{2\ ss}+CuSb_2O_{6\ ss}$	↑
12	0.30	0.70	$SnO_2+CuSb_2O_6$	$SnO_2+CuSb_2O_6$	$SnO_2+CuSb_2O_6$	$SnO_{2\ ss}+CuSb_2O_{6\ ss}$	Melted +
13	0.25	0.75	$SnO_2+CuSb_2O_6$	$SnO_2+CuSb_2O_6$	$SnO_2+CuSb_2O_6$	$SnO_{2\ ss}+CuSb_2O_{6\ ss}$	Decomposed ↑
14	0.20	0.80	$CuSb_2O_6$	$CuSb_2O_6$	$CuSb_2O_6$	$CuSb_2O_{6\ ss}$	
15	0.10	0.90	$CuSb_2O_6$	$CuSb_2O_6$	$CuSb_2O_6$	$CuSb_2O_6$	↑
16	0	1	$CuSb_2O_6$	$CuSb_2O_6$	$CuSb_2O_6$	$CuSb_2O_6$	

Table 2
Lattice parameters of $(1-x)$ SnO_2–$xCuSb_2O_6$ mixtures thermally treated at 1100 °C for 3 h

	Tetragonal symmetry			Monoclinical symmetry				
$x_{CuSb_2O_6}$	a_o(Å)≡ b_o(Å)⩽ ±0.002	c_o(Å)⩽ ±0.002	V_0(Å) ⩽±0.002	a_o(Å) ⩽± 0.002	b_o(Å) ⩽± 0.002	c_o(Å) ⩽± 0.002	β (°)	V_o(Å) ⩽± 0.002
Phase assemblage: SnO_2 ss								
0.00	4.73573	3.18632	71.46000					
0.01	4.73505	3.18578	71.42740					
0.06	4.72508	3.17574	70.90281					
0.10	4.72508	3.17030	70.78133					
0.20	4.70117	3.15790	69.79752					
0.25	4.69813	3.14529	69.42418					
Phase assemblage: SnO_2 ss				+		$CuSb_2O_6$ ss		
0.30	4.69484	3.14924	69.41404	4.64401	4.41366	9.85704	90.91	202.015
0.40	4.69652	3.14862	69.45006	4.64338	4.41903	9.83193	90.88	201.720
0.50	4.70068	3.14563	69.50707	4.64670	4.44173	9.77163	90.93	201.654
0.60	4.69493	3.14848	69.39995	4.64870	4.41487	9.74383	90.82	199.956
0.70	4.69477	3.14942	69.41594	4.64517	4.39152	9.80694	91.17	200.014
0.75	4.69484	3.14710	69.36688	4.64695	4.45398	9.78010	90.86	202.400
Phase assemblage:						$CuSb_2O_6$ ss		
0.80				4.64697	4.42729	9.72519	90.98	199.880
0.90				4.63850	4.52129	9.52683	91.07	199.762
1.00				4.63243	4.63587	9.29666	91.12	199.611

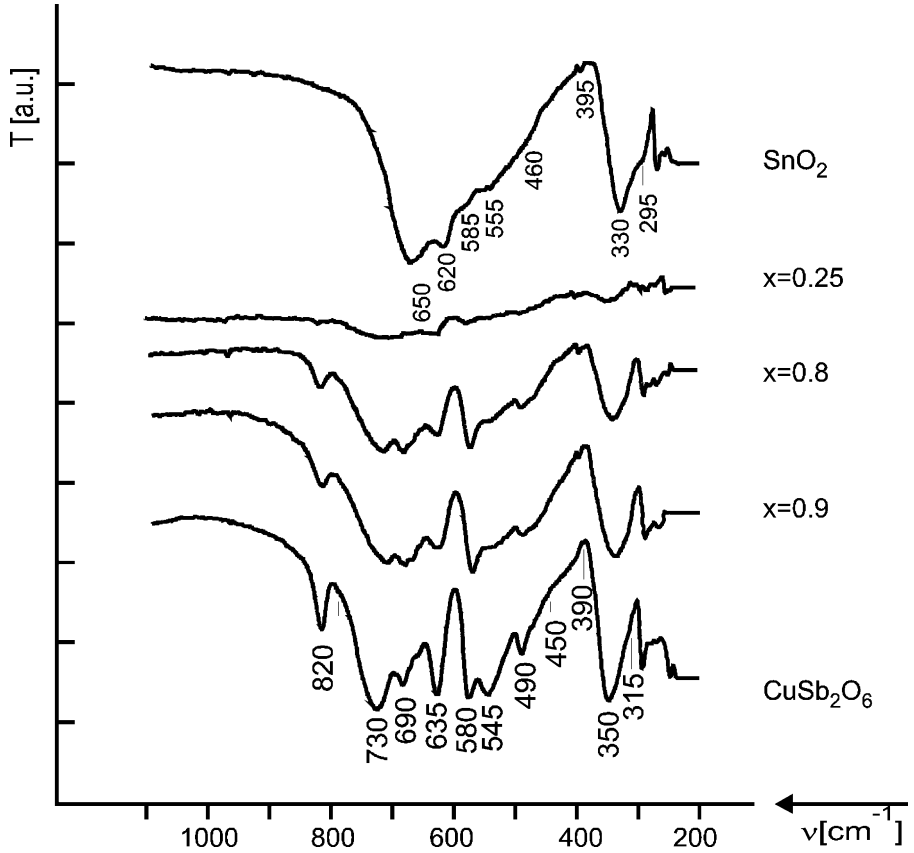

Fig. 4. IR absorbtion spectra of the $(1-x)$ SnO_2–$xCuSb_2O_6$ compositions thermally treated at 1100 °C for 3 h.

Considering the latter observation, the IR spectrum presented in Fig. 4, suggested an advanced crystallinity of SnO_2 used as reference in the present study.

With the formation of $SnO_{2\ ss}$ ($x=0.25$) described by $Sn_{1-x}Cu_{x/3}Sb_{2x/3}O_2$ formalism, an abnormal transmission decrease and the disappearance of the typical IR bands of the components was noticed. Examining the semiconducting properties of $SnO_{2\ ss}$,[19] it is suggested that the phenomenon might be assigned to an increase of the charge carrier concentration, shielding the IR radiation.[12]

4.2. $CuSb_2O_6$ solid solutions

$CuSb_2O_6$ adopts the ideal tetragonal *trirutile* structure only in the high-temperature modification.[20] As can be derived from the present XRD data, the $CuSb_2O_6$ rich end members adopt a monoclinic distorted structure, with β° angle showing a slight deviation from 90° (Table 2). Based upon the cell parameters vs. composition dependence, the solubility limit of SnO_2 in $CuSb_2O_6$ at 1100 °C was estimated to be $x_{SnO_2} \geqslant 0.20$. Similarly, for the *trirutile* type solid solution in accordance with Vegard's rule, the lattice parameters varied with the decreasing of SnO_2 content:

$$a_0 = 4.679 + 0.0005 \cdot x_{SnO_2} \pm 0.002 \text{ Å}$$

$$c_0 = 11.065736 + 0.017544 \cdot x_{SnO_2} \pm 0.002 \text{ Å}$$

For $CuSb_2O_{6\ ss}$, IR spectroscopic investigations (Fig. 4) have been performed. The IR spectrum of pure $CuSb_2O_6$ used as reference is also presented.

All the samples presented in Fig. 4, which were selected from the $CuSb_2O_{6\ ss}$ domain, exhibited defined spectra with easily distinguishable bands relative to the range of 400–800 cm^{-1}, typical for skeletal vibrations of these kind of materials. However, as a general feature of the spectra, the broadness and the reduced intensity of the IR bands suggested a lower degree of crystallinity in the thermally treated samples.

Surprisingly, at the first sight no major changes in the band position and in the intensity distribution are observed when, as evidenced by XRD, $CuSb_2O_6$ based solid solution described as $Cu_{1-x}Sb_{2(1-x)}Sn_{3x}O_6$, is formed ($x=0.8$). However, this observation is readily explained by looking carefully to the size of the ions in the *trirutile* structure,[16] which are of the same order of magnitude. Only the relative intensities of the $CuSb_2O_6$ IR bands are slightly affected by the presence of tin in the *trirutile* lattice, with respect to those of pure $CuSb_2O_6$ (Fig. 4). However, no significant differences are observed. As regards the absorption positions, there seems to be a correlation between the intensity of the bands and the amount of soluble Sn^{4+} from the lattice, since 690 and 490 cm^{-1} bands strongly decreased and 545 cm^{-1} band can be predicted only as a shoulder in the spectra of $CuSb_2O_{6\ ss}$.

By analogy with the results obtained for $MgTa_2O_6$ isomorphous compound,[21] we assigned the IR bands of $CuSb_2O_6$ observed at 730 and 690 cm^{-1} to the vibrations of the oxygen atoms which link the $[Sb_2O_{10}]$ unit to the $[CuO_6]$ octahedra in the *trirutile* type unit cell. The general features of the IR spectra presented in Fig. 4 are the same below 400 cm^{-1}, in the domain where $[CuO_6]$ normal vibration modes can be assigned, in the assumption of a local tetragonally elongated coordination

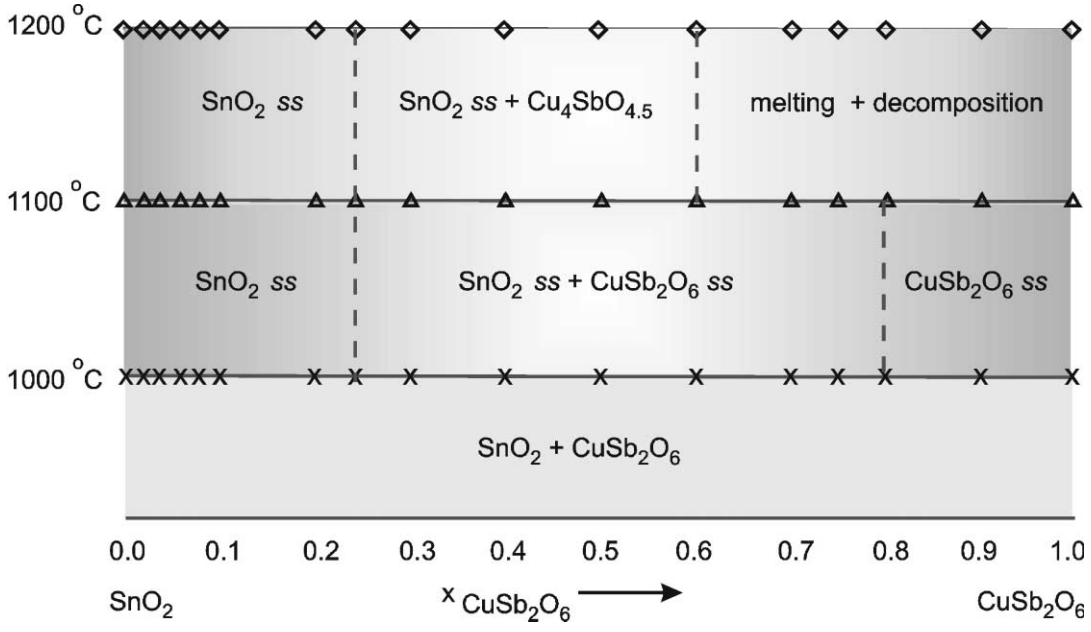

Fig. 5. Subsolidus phase relations in the SnO_2–$CuSb_2O_6$ system.

geometry.[22] According to Husson et al.,[22] the vibrations positioned at 730 and 690 cm^{-1} belong to the degenerate species E_u and E_g. Since only the intensity ratio but not the position of these two bands was modified, the degeneracy is not lifted when $CuSb_2O_6$ based solid solution is formed (Fig. 4). Moreover, in the domain of $CuSb_2O_{6\ ss}$ formation, the average measured value for the magnetic susceptibility of the samples is

$$\chi_{g,25^oC} \approx 3.6\times10^{-6} \quad cm^3\ g^{-1}.$$

This value was found to lie within the reported limits typical for Cu^{2+} ion, unaffected by the presence of diamagnetic ions.[20] As a result of the presented discussion, it is suggested that the Sn^{4+} incorporation into the *trirutile* lattice take place preferentially on Sb^{5+} sites.

Based on the obtained results presented in Table 1, supported by IR investigations, the resulted subsolidus phase relations of SnO_2–$CuSb_2O_6$ system are presented in Fig. 5. Accordingly, the system was divided at 1100 °C into the following three subsolidus domains

$-0 < x \leqslant 0.25$	$SnO_{2\ ss}$ described as $Sn_{1-x}Cu_{x/3}Sb_{2x/3}O_2$
$-0.25 < x < 0.8$	$SnO_{2\ ss} + CuSb_2O_{6\ ss}$
$-0.8 < x \leqslant 1$	$CuSb_2O_{6\ ss}$ described as $Cu_{1-x}Sb_{2(1-x)}Sn_{3x}O_6$

Due to the $CuSb_2O_6$ decomposition and to the presence of the liquid phase extending from the Cu–O system,[15] the phase relationship study becomes more difficult over 1200 °C.

5. Conclusions

The SnO_2–$CuSb_2O_6$ binary system was considered to be representative for the study of SnO_2–Sb_2O_3–CuO ternary system, as concerns the delimiting of different composition areas in accordance with the applications as sensors and catalysts. Two types of solid solutions: $SnO_{2\ ss}$ and $CuSb_2O_{6\ ss}$ with *rutile* and *trirutile* structure respectively, have been obtained by determining the high temperature phase equilibria and phase analysis of the samples.

One has established that SnO_2–$CuSb_2O_6$ is a pseudobinary system with solid solubility limit of the end members.

As regards the composition dependence, the measured lattice parameters of the obtained solid solutions obeyed Vegard's rule. The $CuSb_2O_6$ rich end members adopted a monoclinic distorted structure with β° angle showing a slight deviation from 90°.

From the extent of the modifications of the IR absorption bands, performed on the obtained $Sn_{1-x}Cu_{x/3}Sb_{2x/3}O_2$ and $Cu_{1-x}Sb_{2(1-x)}Sn_{3x}O_6$ mixed crystals, it was established that the Sn^{4+} incorporation might take place preferentially on Sb^{5+} sites.

Acknowledgements

The author wishes to express her gratitude to Professor Joanna Groza from UCD for many helpful discussions. For the experimental work, financial supporting of the USA National Science Foundation (NSF International Supplement #9940988) is gratefully acknowledged.

References

1. Zaharescu, M., Mihaiu, S., Zuca, St. and Matiasovsky, K., Contribution to the study of SnO_2-based ceramics. Part I. High temperature interactions on tin (IV) oxide with antimony (III) oxide and copper (II) oxide. *J. Mater. Sci.*, 1991, **26**, 1666–1672.
2. Varela, J. A., Gouveau, D., Longo, E., Dolet, N., Onillon, M. and Bonnet, J. P., The effect of additives on the sintering of tin oxide. *J. Solid State Phenom.*, 1992, **25–26**, 259–268.
3. Göpel, W. and Schierbaum, K. D., SnO_2 sensors: current status and future prospects. *Sensors and Actuators B*, 1995, **26–27**, 1–12.
4. Pianaro, S. A., Bueno, P. R., Longo, E. and Varela, J. A., Electric properties of a SnO_2 based Varistor. *Ceram. Intern.*, 1999, **25**, 1–6.
5. Scarlat, O., Mihaiu, S. and Zaharescu, M., Semiconducting materials in the SnO_2–CuO system.. In *Proceedings on the International Conference on Semiconductors*, 22nd edn., Vol. 1., Sinaia, Romania, 1999, pp. 401–404.
6. Ramos, E., Isasi, J., Haitan, E. and Veiga, M. L., Synthesis and structural characterisation of antimony (V) mixed oxides with rutile and trirutile-type structure. *An. Quim.*, 1991, **87**, 966–975.
7. Byström, A., Hök, B. and Mason, B., The crystal structure of zinc metaantimonate and similar compounds. *Ark. Kemi, Mineral Geol.*, 1941, **15B** (4), 1–8.
8. Shimada, S., Kodaira, M. and Matsushita, T., Preparation and characterisation of a new copper antimony oxide $Cu_9Sb_4O_{19}$. *J. Solid State Chem.*, 1985, **59**, 237–241.
9. Shimada, S., Mackenzie, K. J. D., Kodaira, K., Matsushita, T. and Ishii, T., Formation of new copper antimony oxides by solid state reactions between $CuSb_2O_6$ and CuO under atmospheric and high pressure. *Thermochim. Acta*, 1988, **133**, 73–76.
10. Shimada, S. and Mackenzie, K. J. D., Solid-State reactions in the system Cu–Sb–O: formation of a new copper (I) antimony oxide. *Thermochim. Acta*, 1982, **56**, 73–82.
11. Ionescu-Scarlat, O., Marchidan, R., Mihaiu, S. and Zaharescu, M. Solid state reactions in the Sn–Sb–Cu–O system studied by IR Spectrometry. In *Key Engineering Materials*, Vols. 132–136. Trans. Tech. Publications, Switzerland, 1997, pp. 848–852.
12. Zaharescu, M., Scarlat, O., Mihaiu, M. S. and Marchidan, R., IR spectroscopy in materials study from Sn–Sb–Cu–O system. *Revue Romaine de Chimie*, 2001, **10**(46), 41–47.
13. Stan, M., Mihaiu, S., Crisan, D. and Zaharescu, M., Subsolidus equilibrium in the Cu–Sb–O system. *Eur. J. Solid State Inorg. Chem.*, 1998, **35**, 243–254.
14. Mihaiu, M. S., Scarlat, O., Radovici, C. and Zaharescu, M., Solid state reactions in the SnO_2–$CuSb_2O_6$ pseudobinary system. In *Proceedings of the 13th Conference on Glass and Ceramics*, ed. B. Samuneva, S. Bacharov, I. Gutzov and Y. Dimitriev. Publishing House Science Invest, Sofia, Bulgaria, 1999, pp. 75–80.
15. Hallstedt, B., Risold, D. and Gauckler, L. J., Thermodynamic assessment of the copper–oxygen system. *J. Phase Equilibria*, 1994, **15**(5), 483–499.

16. Shannon, R. D., Revised effective ionic radii and systematic studies of interatomic distances in halides and chalcogenides. *Acta Cryst*., 1976, **A32**, 751–766.
17. Bordoni, S., Castellani, F., Cavani, F. and Trifiro, F., Nature of vanadium species in SnO_2–V_2O_5 based catalysts. *J. Chem. Soc. Faraday Trans*., 1994, **90**(19), 2981–3000.
18. Xie, C., Zhang, L. and Mo, C., Characterization of Raman spectra in nano-SnO_2 solids. *Phys. Status Solidi*, 1994, **A141**, 59–61.
19. Mihaiu, S., Scarlat, O., Aldica, Gh. and Zaharescu, M., SnO_2 electroceramics with various additives. *J. Eur. Ceram. Soc*., 2001, **21**, 1801–1804.
20. Nakua, A., Yun, H., Reimers, J. N., Greedan, J. E. and Stager, C. V., Crystal structure, short-range and long range magnetic ordering in $CuSb_2O_6$. *J. Solid State Chem*., 1991, **91**, 105–112.
21. Rocchiccioli-Deltcheff, C., Depuis, T., Franck, R., Harmelin, R. F. and Harmelin, M., Infrared absorption spectra of niobates, tantalates and antimonates of the rutile structure. *J. Chim. Phys. Physico-Chim. Biologique*, 1970, **67**(11–12), 2037–2044.
22. Husson, E., Repelin, Y. and Brusset, H., Spectres de vibration et calcul du champ de force des antimonates et des tantalates de structure trirutile. *Spectrochim. Acta*, 1979, **35A**, 1177–1187.